Electrochemical impedance measurement of prostate cancer cells using carbon nanotube array electrodes in a microfluidic channel

2007 Nanotechnology 18 465505

(http://iopscience.iop.org/0957-4484/18/46/465505)

IOP PUBLISHING NANOTECHNOLOGY
Nanotechnology **18** (2007) 465505 (7pp) doi:10.1088/0957-4484/18/46/465505

Electrochemical impedance measurement of prostate cancer cells using carbon nanotube array electrodes in a microfluidic channel

YeoHeung Yun[1], **Zhongyun Dong**[2], **Vesselin N Shanov**[3] **and Mark J Schulz**[1]

[1] Smart Materials Nanotechnology Laboratory, Department of Mechanical Engineering, University of Cincinnati, Cincinnati, OH 45221, USA
[2] Department of Internal Medicine, Hematology-Oncology Division, College of Medicine, University of Cincinnati, Cincinnati, OH 45267, USA
[3] Smart Materials Nanotechnology Laboratory, Department of Chemical and Materials Engineering, University of Cincinnati, Cincinnati, OH 45221, USA

Received 31 July 2007, in final form 22 September 2007
Published 12 October 2007
Online at stacks.iop.org/Nano/18/465505

Abstract
Highly aligned multi-wall carbon nanotubes were synthesized in the shape of towers and embedded into fluidic channels as electrodes for impedance measurement of LNCaP human prostate cancer cells. Tower electrodes up to 8 mm high were grown and easily peeled off a silicon substrate. The nanotube electrodes were then successfully soldered onto patterned printed circuit boards and cast into epoxy under pressure. After polishing the top of the tower electrodes, RF plasma was used to enhance the electrocatalytic effect by removing excess epoxy and activating the open end of the nanotubes. Electrodeposition of Au particles on the plasma-treated tower electrodes was done at a controlled density. Finally, the nanotube electrodes were embedded into a polydimethylsiloxane (PDMS) channel and electrochemical impedance spectroscopy was carried out with different conditions. Preliminary electrochemical impedance spectroscopy results using deionized water, buffer solution, and LNCaP prostate cancer cells showed that nanotube electrodes can distinguish the different solutions and could be used in future cell-based biosensor development.

(Some figures in this article are in colour only in the electronic version)

1. Introduction

Electrochemical impedance has been used broadly for human body measurements down to individual DNA. Especially important is that impedance measurement enables detection of cells in buffer solution, cell–cell interactions and cell–matrix interactions caused by the environment, cytotoxicity or drug delivery [1–16]. The electrical conductivity and impedance of biological materials has been investigated over the past century using conventional electrodes [2–4]. Recently, with the advance of nanotechnology, electrochemical impedance measurement using nanoelectrodes offers advantages such as reduced double layer capacitance, fast convergence to a steady-state signal, enhanced current density arising from increased mass transport at the working electrode interface, low detection limits and improved signal-to-noise ratios [5]. In particular, ordered arrays of carbon nanotubes have been studied rigorously [6–11]. However, fabrication problems associated with carbon nanotubes still need to be addressed in order to make practical devices. For example, fabrication processes should be simplified and oriented to specific applications.

The present paper reports nanoelectrode array development and preliminary testing with prostate cells. First, high

density multi-wall carbon nanotube (MWCNT) arrays up to 8 mm tall were synthesized using water-assisted chemical vapor deposition (CVD). The MWCNT tower was peeled off from the Si substrate and soldered onto pre-patterned printed circuit boards (PCBs). This simplified method enabled contacting the nanotube electrically to metal substrates. After casting into epoxy, the tops of the MWCNT array nanoelectrodes were polished and activated using a radiofrequency (RF) plasma treatment. Furthermore, electrochemical deposition of Au on the activated nanotube sites was done to control the space between individual electrodes. Also the electrodeposition of gold on the activated nanotube enables self-assembly monolayers with different functional groups and further bioconjugation. These processes also offer several advantages, which include mass production and control of the spacing of the electrodes. The optimization of spacing between electrodes can maximize radial diffusion which will increase sensitivity. Cyclic voltammetry and electrochemical impedance spectroscopy (EIS) were used to characterize each step of the fabrication process. Electrochemical Impedance characterization of nanotube electrodes under a fluidic channel was performed using different solutions with LNCaP prostate cancer cells.

2. Experimental set-up

2.1. Synthesis of carbon nanotube towers

Our group previously reported the synthesis of carbon nanotube arrays using a water-assisted chemical vapor deposition process [12]. Briefly, an electron-beam evaporator was used to deposit a 10 nm thick Al film on a Si/SiO_2 wafer. The film was then oxidized to produce Al_2O_3. Then, iron catalyst was deposited through a shadow mask on the $Si/SiO_2/Al_2O_3$ substrate. The nanotube array was then synthesized by thermal chemical vapor deposition (CVD) in a horizontal 2 in EasyTubeTM (ET1000, FirstNano) furnace. Argon, ethylene, water and hydrogen were used for deposition of the carbon nanotubes. The synthesized nanotube arrays were characterized by environmental scanning electron microscopy (ESEM).

2.2. Device fabrication

Figure 1 shows the schematic diagram of the nanotube electrode (tower 1 mm diameter). First, the carbon nanotube (CNT) tower was peeled off from the Si substrate using tweezers. The CNT tower was placed on a Cu patterned printed circuited board (PCB). A Kopper Clad Board coated with dry film photoresist (D&L Product, Inc.) was used to pattern the electrode, and ferric chloride was used for etching the copper. To assemble the CNT tower onto the PCB, heat was applied to the CNT tower and patterned Cu film causing the solder to melt and be drawn into the CNT array by wetting action. The eutectic alloy of 63% tin and 37% lead was used as a solder. The 8 mm long CNT tower was successfully soldered onto the PCB. After cooling to room temperature, the whole component was immersed in epoxy. Resin 862 and EPICURE curing agent W were used for the nanotube epoxy composite [5, 10]. After casting in epoxy, the top section of a CNT tower was polished using a Vibromat polisher (Buehler). The surface of the nanotube array–composite electrode was

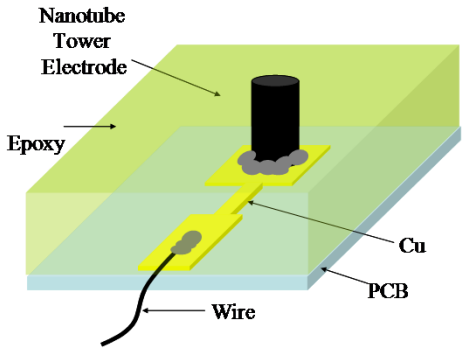

Figure 1. Schematic of a nanotube tower electrode.

polished with different sizes of diamond abrasive (Microid Diamond Compound) from 9, to 3 to 0.5 μm with a 5 N constant force [6, 7]. Polishing was done for 5 min at each step at 150 RPM. Then the samples were rinsed with fresh acetone spray and immediately air-dried.

After polishing the nanotube array–epoxy composite, reactive ion etching (RIE) was used to remove excess epoxy and open the nanotube tips. The plasma mass flow rate was set to 80 standard cubic centimeters per minute (SCCM) with 20% oxygen and the treatment was performed for 2 min at a power of 50 W. After rinsing with acetone, methanol and H_2O, the nanotube array was immersed in hydrogen tetrachloroaurate solution diluted with hydrochloric acid (Aldrich) for electrodeposition of Au with an applied constant potential and different deposition times. Prior to use, the resulting gold coated electrode was first thoroughly rinsed with methanol and water, then dried under a stream of nitrogen.

The upper layer of a fluid channel was made using PDMS (Sylgard 184 PDMS, Dow Corning) [9]. SU-8 photoresist (S2100) and developer from MicroChem were used to make a mold on Si. The SU-8 photoresist was spin-coated (1000 rpm, 30 s) and soft-baked on a hot plate (65 °C, 30 min, followed by 95 °C, 30 min). The SU-8 coated Si was exposed through a photomask with a Solitec mask aligner (40 mW cm^{-2}, 30 s). Postbake was done on a hotplate (65 °C, 1 min, followed by 95 °C, 3 min). The final sample was immersed into SU-8 developer for 30 min. The final master was cleaned with isopropyl alcohol and stored for future use. The thickness of the features was 150 μm as confirmed by profilometry.

The patterned master was bonded to an aluminum mold. PDMS base and curing agent were mixed thoroughly (10:1 by mass), poured onto the master and then degassed under vacuum until bubbles disappeared. Then the whole assembly was cured in an oven (80 °C, 2 h) and cooled to room temperature. PDMS was gently peeled from the master and cut for a fluidic channel. The top of a hypodermic needle was trimmed and used as a punch to make holes for the inlet, outlet and Pt electrodes. A Pt electrode (0.5 mm diameter) was inserted though a hole in the PDMS and sealed using UV curing adhesive (Loctite 3301).

Figure 2 shows a cross section of the final fabricated device for electrochemical impedance measurement. The top PDMS and bottom CNT electrode parts were bonded using UV adhesive. First the adhesive was spread smoothly onto the PDMS part and the two parts were bonded together using a microscope to align the electrodes. An adjustable micrometer

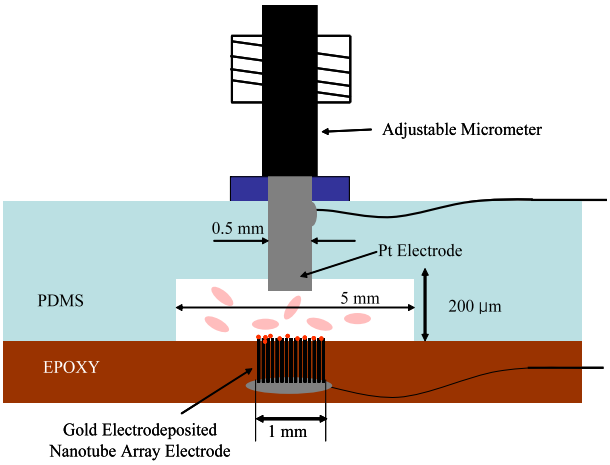

Figure 2. Schematic representation of a microfabricated flow cell with an adjustable gap electrode.

was attached on top of the final device to control the electrode gap.

2.3. Cell culture

Cells were maintained at 37 °C in 5% CO_2 as a monolayer culture in minimum essential medium (MEM) supplemented with 10% fetal bovine serum FBS, nonessential amino acids, sodium pyruvate, vitamin A and glutamine (CMEM). Cells in their exponential growth phase were harvested by a 1–5 min treatment with a 0.25% trypsin–0.02% EDTA solution. The flasks were tapped to detach the cells into CMEM and gently agitated to produce single-cell suspensions. The cells were washed and resuspended in Hanks' balanced salt solution (HBSS). Only suspensions of single cells with viability exceeding 95% (ascertained by trypan blue exclusion) were used.

2.4. Electrochemical characterization procedure

In order to evaluate the electrochemical properties of a nanotube array electrode, cyclic voltammetry and electrochemical impedance spectroscopy were performed using three-electrode cells, with the nanotube electrode as the working electrode, an Ag/AgCl used as the reference electrode and a platinum wire as the counter electrode. CV was carried out using a Bioanalytical Systems (BAS, West Lafayette, IN) analyzer operated by an Epsilon system with a C3 cell stand in a Faraday cage. EIS measurements were performed using a Gamry Potentiostat (Model: PCI4/750) coupled with EIS (Gamry, EIS300) software. All reagents were prepared fresh daily in deionized water.

3. Results and discussions

Figures 3(a)–(c) show ESEM images of nanotube towers at different magnifications. The towers were grown with the assistance of water while fixing the other growth conditions: 200 SCCM of H_2 flow, 200 SCCM of C_2H_4 flow and a 750 °C growth temperature. The $Fe/Al_2O_3/SiO_2/Si$ substrate is cut into 5 mm squares from one wafer and Fe is patterned on a 1 mm circle with 1 mm spacing between the blocks. With the increase of growth time, the length of the CNT arrays increases for up to 3 h.

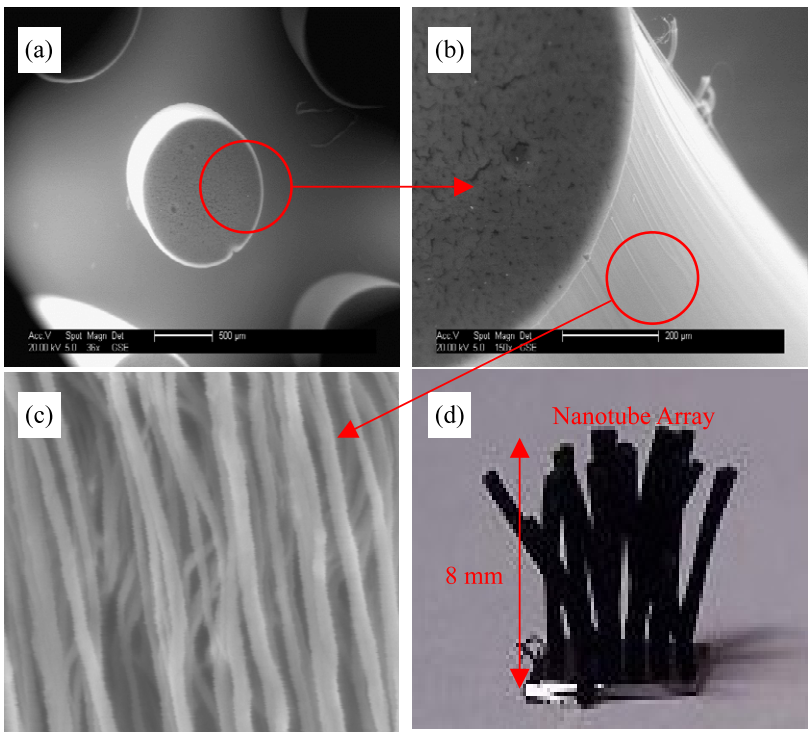

Figure 3. ESEM images of aligned multi-wall carbon nanotube patterned arrays: (a) one bundle of nanotubes called a tower; (b) top view of a nanotube tower; (c) high resolution side view of a nanotube tower; (d) picture of an 8 mm tall MWCNT patterned array on the Si wafer. Growth conditions are: 200 SCCM of H_2, 200 SCCM of C_2H_4, 200 SCCM bubbler and a 750 °C growth temperature.

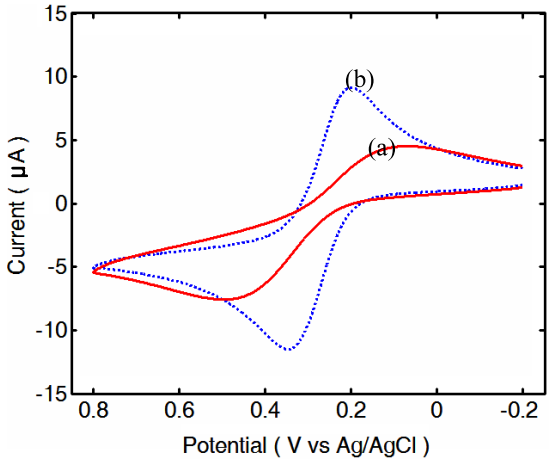

Figure 4. CV of 6.0 mM $K_3Fe(CN)_6$ in 1.0 M KNO_3 at 100 mV s^{-1}: (a) before and (b) after plasma treatment. Background current was not subtracted.

The MWCNT array has high density without many impurities, which is ideal for further application development. Adhesion to the substrate is weak and the MWCNT array is easily peeled off. One bundle of a MWCNT array block can be easily removed from the array using tweezers without damage. Figure 3(d) shows a 8 mm tall MWCNT patterned array on a Si wafer. Each tower (1 mm × 1 mm) of the patterned array contains around 50 million nanotubes. The nanotube average diameter is 20 nm and the aspect ratio is 200 000. The surface area of each tower (for an average 20 nm diameter, 8 mm length nanotube) is 2500 mm^2. In order to measure the resistivity of the nanotube tower, we cast a nanotube tower in epoxy and polished both ends of the nanocomposite, and wired the electrode using conductive epoxy. Volume resistivity was around 0.11 Ω cm.

Figure 4 shows the cyclic voltammograms for the reduction of 6.0 mM $K_3Fe(CN)_6$ (in 1.0 M KNO_3 as a supporting electrolyte) at a nanotube electrode before and after plasma treatment. A significant increase in peak current with a smaller peak separation voltage, $\Delta E_p = 0.18$ V, was obtained after plasma treatment. Also, the reaction after plasma treatment has better electron transfer at the electrode. Probably the opened-end and protruding nanotube after plasma treatment provides effective electrocatalytic sites since electron transport through the edge plane of the nanotube is primarily responsible for the conductivity. After activating the nanotube electrodes, further electrodeposition of gold was done to control the density of the electrodes. More than 30 samples were tested, and peak current and separation voltage did not deviate more than 3% after treating with RF plasma.

Figure 5 shows the magnitude and phase plot of electrochemical impedance with different solutions (a)–(c) between the electrodes. Individual curves are the averages of three frequency sweeps. The impedance results reflect properties of the electrode's geometry and current path in the solution. Larger magnitudes in figure 5(a) correspond to a milli-Q solution, and show lower ionic concentration and a constant magnitude at a higher frequency range. On the other hand, the smaller magnitude of electrical impedance after contacting each electrode was acquired with a smaller phase up to 10 kHz as shown in figure 5(c). These results show typical contact resistance behavior. The impedance magnitude between milli-Q water and direct electrical contact is around two orders of magnitude different. The magnitude of impedance of DI water is a linear response with a constant slope (on a log scale) over the frequency range of 1 Hz to 1 kHz. A simple resistivity test showed that the resistivity of milli-Q was 18 MΩ cm and the resistivity of distilled water was 1 MΩ cm. These resisitivity results explain why EIS created a difference between DI and milli-Q water.

Figure 6 shows the complex electrochemical impedance with different solutions between the electrodes. In the case of the direct contact of each electrode, a compressed semicircle with low magnitude shows the combination of resistance and capacitance at the contact areas. Even though we did not show the results, with the increase of pressure on each electrode, the diameter of the semicircle kept decreasing.

Figure 7 shows the Bode plot of HBSS and LNCaP cells with different incubation times. When LNCaP cells attach and spread on the surface of individual electrodes they behave essentially like insulating particles which hinder unrestricted current flow from the electrode into the bulk electrolyte [11–16]. However, when the applied frequency is

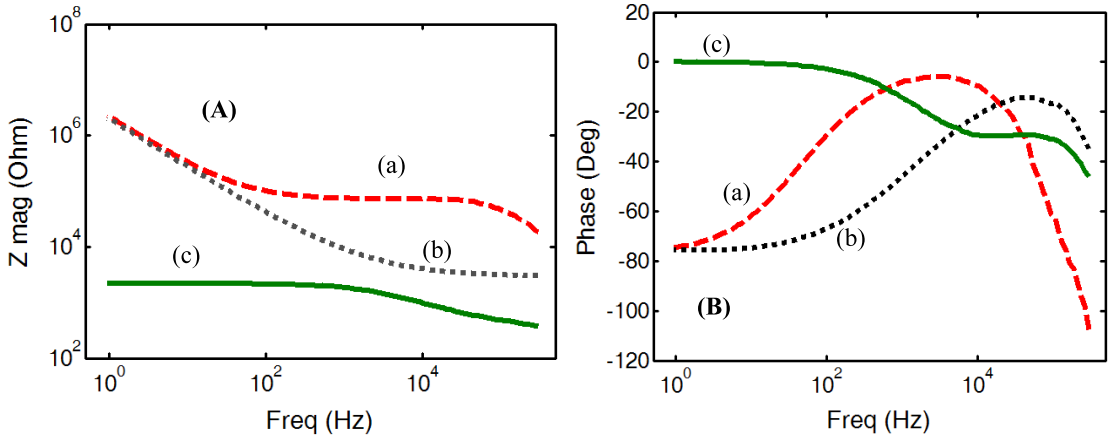

Figure 5. Magnitude (A) and phase (B) plot of electrochemical impedance with: (a) milli-Q water; (b) DI water; and (c) contacting electrodes.

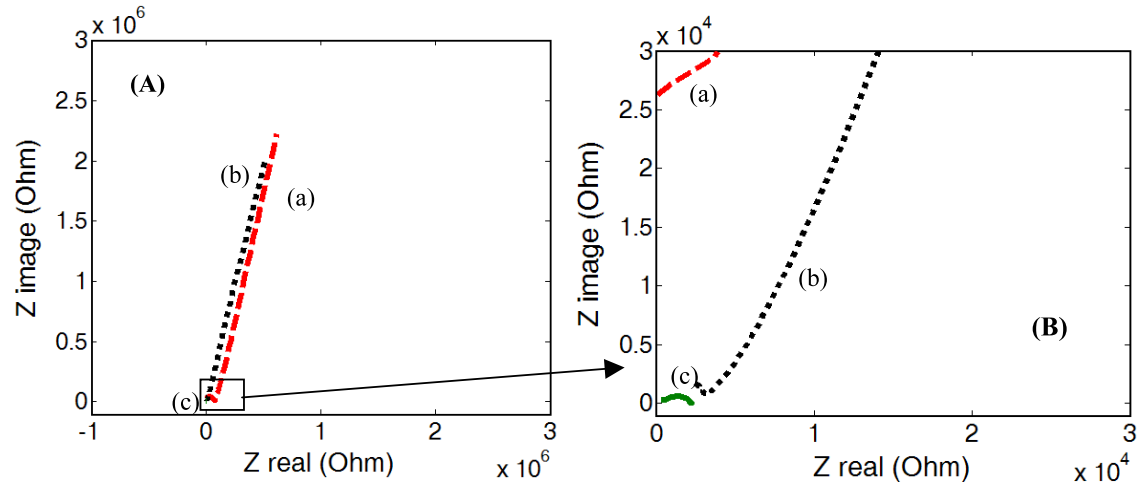

Figure 6. The complex impedance (A) with magnified plot (B) with: (a) milli-Q water; (b) DI water; and (c) contacted electrodes.

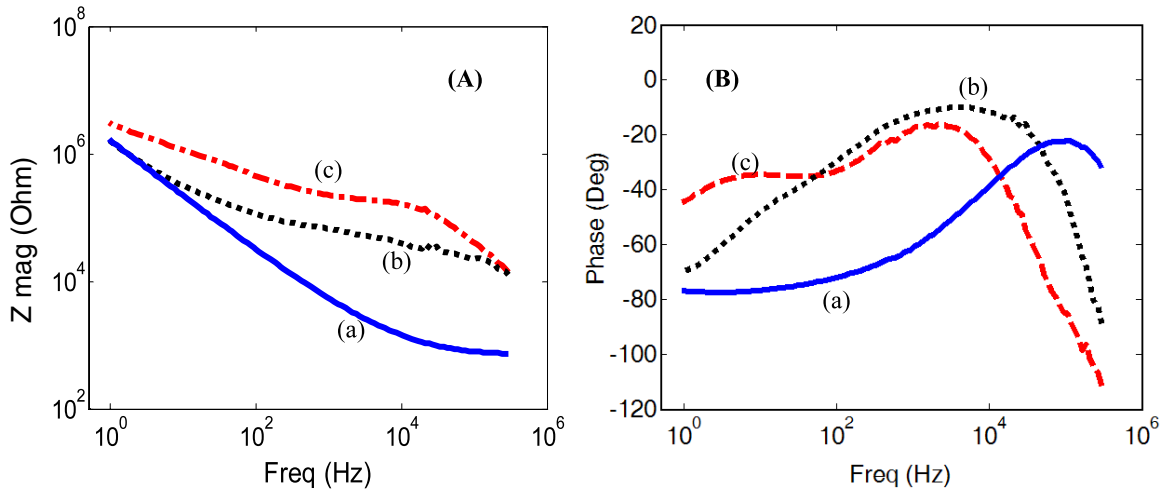

Figure 7. Magnitude (A) and phase (B) plot of electrochemical impedance in: (a) HBSS; and then HBSS with LNCaP with different incubation times: (b) 5 min; and (c) 2 h.

high enough, current can penetrate the plasma membrane and cross the cell layer. In general, we can define three frequency regions called α, β, γ dispersions [1]. As shown in figure 7, the impedance of LNCaP prostate cells increased especially at 100–1000 Hz compared to the HBSS. Probably the capacitance of the LNCaP cells blocks the current from 100 to 1000 Hz. Another difference between the HBSS and LNCaP prostate cells is the phase angles, which are more capacitive with the increase of incubation time. Probably LNCaP prostate cells form a tight contact and cover the individual electrodes, which blocks ion movement. Therefore, the increase of resistance and capacitance of the individual electrode surfaces creates a large difference compared to the HBSS solution. This phenomenon can be seen clearly on the Nyquist plot in figure 8, showing that the diameter of the semicircle at high frequency is increasing with incubation time.

Based on figures 7 and 8, the equivalent circuit model as shown in figure 9 was considered for electrical cell–substrate impedance sensing [12–16]. As shown in figure 7, the HBSS has only one double layer capacitance, which can be modeled as a constant phase element, CPE with a solution resistance, R_u. Extracted parameters were CPE $= 0.134$ μS, $\alpha = 0.83$ and $R_u = 950$ Ω. A higher value of α is indicative of the closeness of the constant phase element to an ideal capacitor ($\alpha = 1$).

Since the solution resistance represents the bulk properties of the electrolyte solution and the LNCaP cells settled on the electrode's surface, solution resistance did not change much. On the other hand, the cell layer capacitance C_{cl} and cell layer resistance R_{cl} affect the interface property of the electrode/electrolyte due to insulating or coating the surface by LNCaP cells. As shown in table 1, C_{cl} and R_{cl} are sensitive to the addition of LNCaP prostate cells. The value of cell membrane capacitance is about 20 pF cm^{-2} [1] and individual cells have hundreds of fF depending on the cell condition [1]. In order to measure the cell membrane capacitance, a patch clamp technique poking or penetrating the cell with an electrode is normally needed. However, our suggested method can measure the capacitance of hundreds of cells simultaneously without damaging the cells. Further studies are needed since electrodeposition of gold on the activated nanotube enables self-assembly of monolayers and

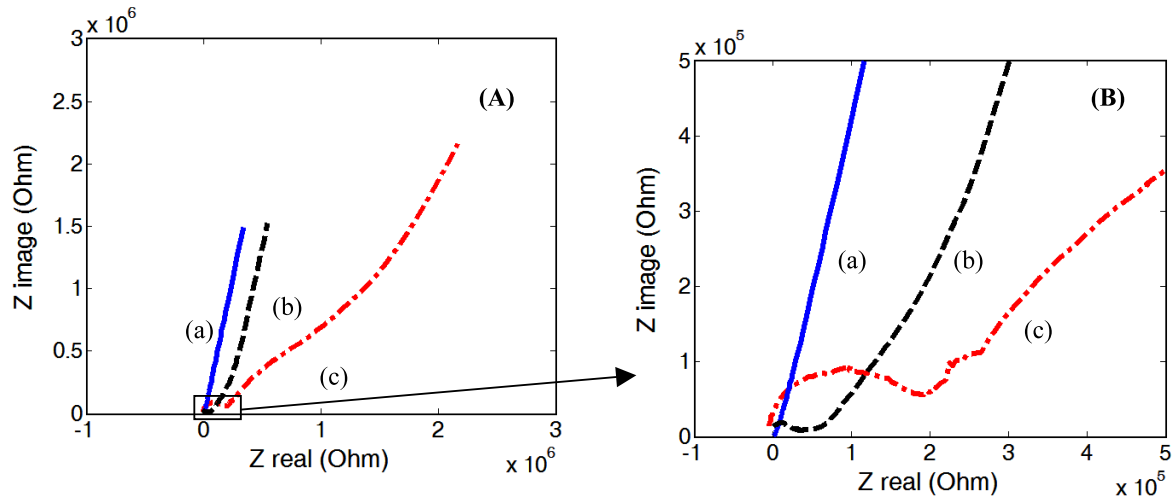

Figure 8. The complex impedance (A) with magnified plot (B) of electrochemical impedance in: (a) HBSS; and then HBSS with LNCaP with different incubation times: (b) 5 min; and (c) 2 h.

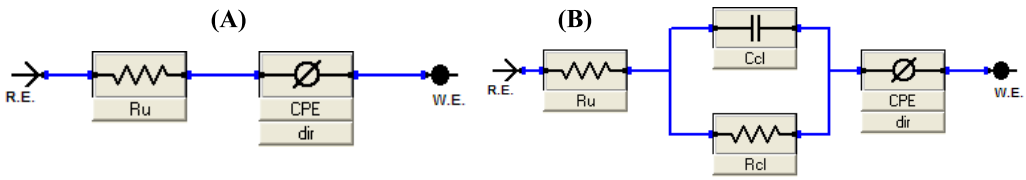

Figure 9. Equivalent circuit model of (A) HBSS and (B) LNCaP. R_u is a solution resistance, CPE is a constant phase element, C_{cl} is a cell layer capacitance and R_{cl} is a cell layer resistance.

Table 1. Estimated parameters for nanotube array-gold electrodes with LNCaP cells.

	CPE (μS)	α	R_u (Ω)	C_{cl} (pF)	R_{cl} (kΩ)
Figure 8(a)	0.134	0.83	950	—	—
Figure 8(b)	0.137	0.75	950	54	35
Figure 8(c)	0.150	0.72	950	200	140

bio-conjugation for future prostate cancer cell separation in blood.

4. Conclusions

Highly aligned multi-wall carbon nanotubes were synthesized in the shape of towers and embedded into fluidic channels as electrodes for impedance measurement of prostate cancer cells. Patterned MWCNT towers up to 8 mm high were successfully grown. Simple fabrication processes, including a printed circuit board technique and electrodeposition, were developed for future mass production. Cyclic voltammetry of plasma-treated nanotube electrodes showed that activation of carbon nanotubes and electrodeposition of Au particles on plasma-treated tower electrodes effectively controlled the density of the electrodes. The gold coated nanotube electrodes were embedded into a polydimethylsiloxane (PDMS) channel and electrochemical impedance results using deionized water, buffer solution and LNCaP prostate cancer cells showed that the nanotube electrode can characterize different solutions which suggests its use as a cell-based biosensor. Gold functionalized nanotube array electrodes will be useful for further bio-conjugation such as antibodies, aptemers and special receptors to detect specific cancer cells.

References

[1] Sverre G and Orjan M 2000 *Bioimpedance and Bioelectricity: Basic* (New York: Academic)
[2] Kissinger P T and Heineman W R 1996 *Laboratory Techniques in Electroanalytical Chemistry* 2nd edn, rev. and expanded (New York: Dekker)
[3] Sohn L L, Saleh O A, Facer G R, Beavis A J, Allan R S and Notterman D A 2000 Capacitance cytometry: measuring biological cells one by one *Proc. Natl Acad. Sci. USA* **97** 10687–90
[4] Wightman M W 1998 Voltammetry with microscopic electrodes in the new domains *Science* **240** 415–20
[5] Yun Y H, Shanov V, Tu Y, Schulz M J, Yarmolenko S, Neralla S, Sankar J and Subramaniam S 2006 A multi-wall carbon nanotube tower electrochemical actuator *Nano Lett.* **6** 689–93
[6] Li J, Ng H T, Cassell A, Fan W, Chen H, Ye Q, Koehne J, Han J and Meyyappan M 2003 Carbon nanotube nanoelectrode array for ultrasensitive DNA detection *Nano Lett.* **3** 597–602

[7] Koehne J, Chen H, Li J, Cassell A M, Ye Q, Ng H T, Han J and Meyyappan M 2003 Ultrasensitive label-free DNA analysis using an electronic chip based on carbon nanotube nanoelectrode arrays *Nanotechnology* **14** 1239–45
[8] Hinds B J, Chopra N, Rantell T, Andrews R, Gavalas V and Bachas L G 2004 Aligned multiwalled carbon nanotube membranes *Science* **303** 62–5
[9] Yuzvinsky T D, Fennimore A M, Kis A and Zettl A 2006 Controlled placement of highly aligned carbon nanotubes for the manufacture of arrays of nanoscale torsional actuators *Nanotechnology* **17** 434–8
[10] Yun Y H *et al* 2007 A Nanotube array immunosensor for direct electrochemical detection of antigen–antibody binding *Sensors Actuators* B **123** 177–82
[11] Carlo D D, Wu L Y and Lee L P 2006 Dynamic single cell culture array *Lab on a Chip* **6** 1445–9
[12] Yun Y H, Shanov V, Tu Y, Subramaniam S and Schulz M J 2006 Growth mechanism of long aligned multi-wall carbon nanotube arrays by water-assisted chemical vapor deposition *J. Phys. Chem.* B **110** 23920
[13] Schwan H P 1957 Advances in biological and medical physics *Electrical Properties of Tissue and Cell Suspensions* vol 5 (New York: Academic) pp 147–209
[14] Gascoyne P R, Pethig R, Burt J P and Becker F F 1993 Membrane changes accompanying the induced differentiation of friend marine erythroleukemia cells studied by dielectrophoresis *Biochim. Biophys. Acta* **1149** 119–26
[15] Arndt S, Seebach J, Psathaki K, Galla H J and Wegener J 2004 Bioelectrical impedance assay to monitor changes in cell shape during apoptosis *Biosens. Bioelectron.* **19** 583–94
[16] Giaever I and Keese C R 1993 A morphological biosensor for mammalian cells *Nature* **366** 591–2